Available online at www.sciencedirect.com
ScienceDirect
Journal of Sound and Vibration 311 (2008) 633–651
JOURNAL OF SOUND AND VIBRATION
www.elsevier.com/locate/jsvi

Determination of normal force for optimal energy dissipation of harmonic disturbance in a semi-active device

Paulin Buaka Muanke, Patrice Masson*, Philippe Micheau

G.A.U.S., Mechanical Engineering Department, Université de Sherbrooke, Sherbrooke, Québec, Canada J1K 2R1

Received 15 February 2006; received in revised form 12 September 2007; accepted 20 September 2007
Available online 31 October 2007

Abstract

A semi-active device is presented for vibration control using energy dissipation by dry friction at contact surfaces. The device uses two piezoelectric stack actuators to apply a normal force between a moving mass component and two friction pads. The objective is to adjust the normal force in order to reach the maximal power dissipated. The theoretical optimal normal force is predicted with an analytical model of the device. The normal force generator is modelled using the piezoelectric constitutive equations. The LuGre model is proposed for the dry friction modelling and then reduced to the Coulomb model. The parameters of the spring-mass-damper, force generator and dry friction models were identified experimentally. The dissipated power is obtained from the experimental measurements and presented with respect to the operating parameters (voltage, frequency, excitation force) and the results validate the presented optimal constant normal force to maximize the energy dissipated.

1. Introduction

Semi-active techniques offer several advantages over passive or active techniques for vibration control. These techniques have been implemented with success in many automotive and civil engineering applications especially through viscous friction using electrorheological or magnetorheological fluids [1,2]. However, semi-active control using energy dissipation through dry friction has been relatively less investigated. Most of the applications of dry frictions are seen in large-scale aerospace structures with semi-active dry friction joints [1,3–6] and in the automotive industry with semi-active dry friction suspensions [7–9].

In this work, an approach is presented where dry friction between two surfaces in relative motion is used to control the vibration in structures by energy dissipation. This could be achieved using a number of devices with controlled friction interfaces bonded to a vibrating structure. Although the idea of using dry friction is not new [10], as opposed to actual devices proposed in the literature [7,8] for which the typical dimension is in the order of 30 cm, the ultimate goal of the current research effort is to develop a miniaturized device, in the order of a few millimeters, that could be distributed over a vibrating surface without adding too much mass as it is the case for viscoelastic material or dynamic absorbers [11–16].

*Corresponding author. Tel.: +1 819 821 8000x62152; fax: +1 819 821 7163.
E-mail address: Patrice.Masson@USherbrooke.ca (P. Masson).

0022-460X/$ - see front matter © 2007 Elsevier Ltd. All rights reserved.
doi:10.1016/j.jsv.2007.09.021

Later, it will be showed that even a simplified friction model is adopted for the friction force; both the theoretical analysis and the experimental measurement demonstrate the existence of the optimal constant normal force to maximize the energy dissipated. This is done before any kind of control algorithm is applied. So the study opens the way to work on how to further improve the energy dissipation obtained from the optimal constant normal force by controlling this normal force.

The paper is organized as follows. Section 2 presents the concept behind the device. Section 3 presents the theoretical modelling of the device behavior and its characterization in terms of the power dissipated. In Section 4, experimental results are presented to validate the semi-active device while conclusions are presented in Section 5.

2. The semi-active friction device

The operating principle of the device is relatively simple: a signal (acceleration, velocity or displacement) measured by a sensor is fed to a controller to generate the command signal in order for the actuators to apply a normal force F_N which will press the friction pads on a moving mass component which is in relative motion to the pads. This results in a friction force to be generated at the interface between the moving mass component and the friction pads positioned on both sides of it, such that the host structure vibrating energy is dissipated through friction at this contact interface. Such semi-active device can be modelled as a friction damper consisting of a moving mass supported by springs and dampers as illustrated in Fig. 1(a). The harmonic excitation force is applied to the moving mass and is opposed to the friction force at the contact interface with the friction pads.

To induce friction at the interface, normal forces are applied by piezoelectric stack actuators in order to maintain the contact between the moving mass and the friction pads and those normal forces result from the voltage applied to the piezoelectric stack actuator. The device uses piezoelectric actuators because of their large bandwidth and large forces that can be generated and thus allowing for the use of advanced control strategies. Moreover, piezoelectric material is currently being used in MEMS (Micro-electro-mechanical systems) and this could therefore simplify the miniaturization of the device.

Optimizing the energy dissipated amounts to maximize the work done by the friction force at the interface contact between the surfaces in relative motion. The relation between the normal force and the relative displacement of the moving mass is such that, for the same harmonic excitation force amplitude, a large normal force induces a large friction force which opposes a great resistance which in turn reduces the relative displacement amplitude. In the worst case, a too high normal force will cancel the energy dissipation by sticking of the surfaces. On the other hand, a small normal force induces a small friction force but the relative displacement has a greater amplitude. Again, in the worst case, a too low normal force will release the contact which will, in turn, lead to the cancellation of the friction force. So, to obtain maximal energy dissipated by the friction device, a trade-off must be achieved between the need to have a large friction force and a large relative

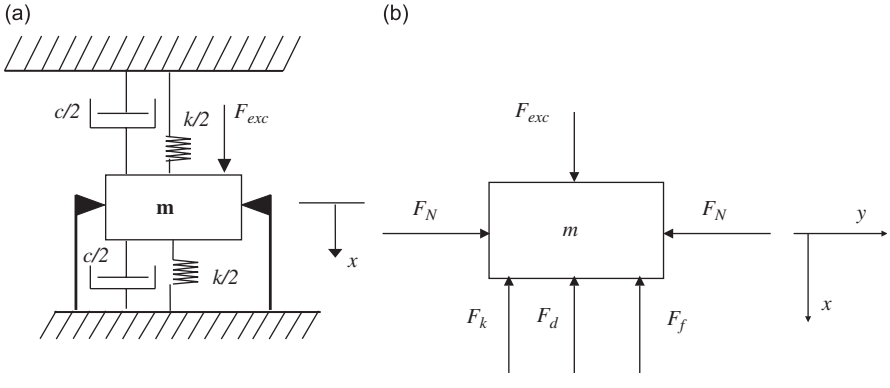

Fig. 1. Semi-active friction device mechanical model with the moving mass (a) and free body diagram with $F_d = c\dot{x}$, the force due to the equivalent viscous damping (b).

displacement. The main difficulty of the control approach involved with this device is to manage this trade-off in the adjustment of the normal force in order to optimize the energy dissipated.

3. Modelling of the semi-active friction device

The dynamic of the semi-active device is represented by a single degree-of-freedom mass-spring-damper system subjected to the friction force. The use of this dynamic equation requires the identification of the mass, the equivalent stiffness and the equivalent viscous damping coefficient of the device. Moreover, as the friction force is also integrated in this model, the parameters of the friction model also need to be identified.

3.1. Modelling of the spring-mass-damper system

Figs. 1(a and b), show, respectively, the simplified model of the moving mass of the semi-active friction device and its free body diagram. The dynamic of the system is represented by the well-known single degree-of-freedom mass-spring-damper system subjected to the friction force given by

$$F_{\text{exc}}(t) - c\dot{x}(t) - kx(t) - F_f(t) = m\ddot{x}(t), \tag{1}$$

where m is the moving mass, x is the relative displacement of the moving mass, k is the equivalent stiffness, c is the equivalent viscous damping coefficient, F_{exc} is the excitation force and F_f is the friction force.

For a harmonic forced vibration at frequency ω, the excitation force $F_{\text{exc}}(t) = F\cos(\omega t + \gamma)$ where F is the amplitude and γ is the phase angle. The analysis of such a system without friction force is well-known and largely developed in the literature [17]. In the remainder of this section, the emphasis is put on the energy dissipated by the friction force during the relative motion. Eq. (1) contains, on the one hand, the device dynamic parameters like the mass, the equivalent stiffness and the equivalent viscous damping coefficient, and on the other hand, the friction parameters in the expression of the friction force F_f.

Once the parameters m, k and c have been identified, the friction force could be estimated using Eq. (1) without a detailed description of the friction model. However, if the friction model is used and its parameters identified, the friction force can be predicted and the estimated value from Eq. (1) can be used to validate the friction model.

For the identification, the mass can be found using a precision balance, and it is useful to obtain the transfer function of the device to identify k and c. Thus, the transfer function between the displacement $x(t)$ of the moving mass and the excitation force $F_{\text{exc}}(t)$ applied to the device is found first by considering that no friction force is applied, i.e. the friction pads are not in contact with the moving mass. With this assumption, Eq. (1) becomes

$$m\ddot{x}(t) + c\dot{x}(t) + kx(t) = F_{\text{exc}}(t). \tag{2}$$

From Eq. (2), the transfer function between the relative displacement and the excitation force is

$$H(s) = \frac{X(s)}{F_{\text{exc}}(s)} = \frac{1/k}{s^2/\omega_n^2 + (2\zeta/\omega_n)s + 1}, \tag{3}$$

where $\omega_n = \sqrt{k/m}$ is the natural frequency, $\zeta = \frac{1}{2}(c/\sqrt{km})$ is the damping coefficient and $(1/k)$ is the static gain of the second-order transfer function. Section 4.2 presents the results for the identification of the dynamic parameters of the device.

3.2. Friction modelling

Friction phenomena are represented by a great variety of friction models with different parameters [10]. Most advanced models exploit velocity dynamics [18]. The general form for these models is

$$F_f = F_N f(\dot{x}, z), \quad \dot{z} = g(\dot{x}, z), \tag{4}$$

where f is a function relating the friction force to the relative velocity $\dot{x}$, z is a variable describing the internal state of friction and g is a function relating the internal state velocity $\dot{z}$ to the relative velocity $\dot{x}$ and the internal state z of the friction.

Canudas de Wit et al. [19] proposed the so-called *LuGre friction model* which belongs to the dynamic velocity class of friction models. This model aims at incorporating all friction nonlinearities (pre-sliding displacement, Stribeck effect, frictional memory, viscous friction, varying break away force) using six parameters. The LuGre friction model equations are recalled in this section and assumptions are then made to simplify the LuGre model to the Coulomb model used in the theoretical and experimental development of this semi-active device.

In the LuGre friction model, the contact between two rigid bodies contact is conceptualized as contact through elastic bristles. When relative motion occurs, the bristles are deflected like elastic spring and damper elements. The proposed model is based on the average behavior of the bristles. The average deflection of the bristles is the internal friction state parameter denoted by z. Within this model, the friction force is expressed by

$$F_f = F_N\left(\sigma_0 z + \sigma_1 \frac{\mathrm{d}z}{\mathrm{d}t} + \sigma_2 \dot{x}\right), \tag{5a}$$

$$\frac{\mathrm{d}z}{\mathrm{d}t} = \dot{x} - \frac{|\dot{x}|}{g(\dot{x})} z, \tag{5b}$$

$$\sigma_0 g(\dot{x}) = F_c + (F_s - F_c)\exp\left(-\frac{\dot{x}^2}{v_s^2}\right), \tag{5c}$$

where σ_0 is the stiffness and σ_1 is the damping coefficient of the bristles, σ_2 is the viscous damping coefficient, F_c is the Coulomb friction force, F_s is the stiction force and v_s is the Stribeck velocity. The function g is positive and depends on many parameters such as material properties, lubrication and temperature. The function $g(\dot{x})$ decreases monotonically from $g(0)$ when $\dot{x}$ increases and this corresponds to the Stribeck effect [19,20]. With this description, the model is thus characterized by six parameters σ_0, σ_1, σ_2, F_c, F_s and v_s. For an implementation of the LuGre model, a state estimator is required since the friction state is not measurable [19].

Assuming steady-state motion, with operating conditions such that $\dot{x} \gg v_s$ and if the viscous friction is neglected with respect to the friction force, Eq. (5a) can be simplified to the equation:

$$F_f = F_N F_c \operatorname{sgn}(\dot{x}) = \mu F_N \operatorname{sgn}(\dot{x}), \tag{6}$$

which is the Coulomb friction model with $F_c \equiv \mu$ where μ is the dynamic coefficient of friction.

All these assumptions and simplifications are useful for the present study since the interpretation of the experimental results will be facilitated by using the Coulomb friction model.

3.3. Theoretical analysis with Coulomb friction model

3.3.1. Approximate solution to the equation of motion

Eq. (6) describes the Coulomb friction model and introduces a nonlinear term in the dynamic equation of motion. An exact solution to the latter can be found for a simple problem but, for more complex problems, an approximate solution has to be considered. The basis of one of the approximate method, known as the "*harmonic balance method*", is to replace the non-linear term $\mu F_N \operatorname{sgn}(\dot{x})$ by a series of harmonic components. But this approximate solution retains the essential qualitative features due to the fact that the first harmonic amplitude in the series development of the friction force is three times the third harmonic amplitude, nine times the fifth harmonic amplitude and so on [17]. Furthermore, the dry contact between the moving mass and friction pads surfaces leads to consider the friction force as the major source of damping in the device, so that the viscous force $c\dot{x}(t)$ is neglected with respect to the Coulomb friction force model F_f in Eq. (1). Then, by assuming the displacement $x(t) = X\cos(\omega t)$, $\dot{x}(t) = -\omega X \sin(\omega t)$, and the Fourier expansion of Eq. (6) is

$$\mu F_N \operatorname{sgn}(\dot{x}) = -\frac{4\mu F_N}{\pi}\sin(\omega t) + \cdots . \tag{7}$$

By considering the first harmonic, Eq. (1) therefore becomes

$$m\ddot{x} + kx - \frac{4\mu F_N}{\pi}\sin(\omega t) = F_{\text{exc}}(t) = F\cos(\omega t + \gamma). \tag{8}$$

After developing, identifying term by term the coefficients of $\sin(\omega t)$ and $\cos(\omega t)$ and rearranging the terms, the following expressions are obtained:

$$X = F\sqrt{1 - \left(\frac{a}{F}\right)^2}\,|H(\mathrm{j}\omega)|, \tag{9}$$

$$\gamma = \tan^{-1}\left(\frac{a}{X}\frac{1/k}{1 - (\omega/\omega_n)^2}\right) \tag{10}$$

with $a = 4\mu F_N/\pi$ and $|H(\mathrm{j}\omega)| = (1/k/|1 - (\omega/\omega_n)^2|)$ is the magnitude of the transfer function.

The phase shift γ is to be understood as the phase shift between the displacement of the mass component and the applied excitation force due to the dynamics of the system and the friction force. To find a solution to Eq. (9), one needs to find the amplitude of the displacement X and the phase shift γ. These two parameters have to be determined from Eq. (9) to Eq. (10) in two steps. Once the amplitude X is computed from Eq. (9), then Eq. (10) can be used to calculate the phase shift γ.

Eq. (9) presents a singularity, as $X \to \infty$ with $\omega \to \omega_n$, this means that friction does not prevent infinite amplitudes from occurring at resonance in this simple case. Friction isolators or dissipators are not useful by themselves to attenuate the resonance peaks. Viscous damping should be also considered for this purpose [17,21]. Eq. (9) shows also that, for the same harmonic excitation force, the amplitude of displacement X is a function of the parameter a which is itself a function of the normal force and therefore of the friction force. Eq. (9) has real value only if $F > a$, which corresponds to the case of a relative motion of the moving mass. For $F < a$, there is no real value, and this case corresponds to the sticking of the moving mass and occurs when excitation force is smaller than the friction force.

3.3.2. Power dissipated by the Coulomb friction force

The energy dissipated during one cycle corresponds to the work done by the friction force during this cycle and in the case of the Coulomb friction model with harmonic force excitation is given by

$$\Delta W = \oint_{x(t_0)}^{x(t_0+T)} F_f\,\mathrm{d}x = \int_{t_0}^{t_0+T} F_f\dot{x}\,\mathrm{d}t = 4\mu F_N X \tag{11}$$

with the period $T = 2\pi/\omega$, $\dot{x}$ is the relative velocity, X is the maximal amplitude displacement given by Eq. (9) and t_0 is the time when the cycle starts. The power dissipated is therefore given by

$$P_{\text{dis}} = \frac{\Delta W}{T} = \frac{4\mu F_N X}{T} = \frac{a\omega}{2}X. \tag{12}$$

Eq. (12) shows that the power dissipated is large if the displacement is large and/or the normal force is large too. One should keep in mind that if the normal force is increased, the friction force is also increased and a greater resistance is presented to the motion that will reduce the amplitude of displacement in accordance with Eq. (9). The problem is, for a given harmonic excitation force, to find the appropriate normal force to obtain the maximal power dissipated by friction. With F kept constant, this problem can be formulated as to find the optimal value of the parameter a denoted a_{opt} which leads to the maximal power dissipated. Using the expression of X from Eq. (9) into Eq. (12), the power dissipated takes the following form:

$$P_{\text{dis}} = aF\left(\frac{\omega}{2}\right)\sqrt{1 - \left(\frac{a}{F}\right)^2}\,|H(\mathrm{j}\omega)|. \tag{13}$$

Eq. (13) vanishes for $a = 0$ which is the case of no normal force applied ($F_N = 0$) and for $a = F$ which is the case of no relative motion ($F_N \geqslant (\pi/4\mu)F$). In this latter case, the normal force is larger than the excitation force consequently there is sticking and no power is dissipated. The optimal value of the parameter a which leads to the maximal power dissipated is between $a = 0$ and $a = F$, is related to the optimal normal force and

is given by

$$\left.\frac{dP_{dis}}{da}\right|_{a_{opt}} = 0 \Longrightarrow a_{opt} = \frac{F}{\sqrt{2}}. \tag{14}$$

When the parameter a is normalized with respect to the amplitude of the excitation force F, the normalized optimal value of the parameter a in Eq. (14) is as follows:

$$a_{opt,\,norm} = a_{opt}/F = \frac{1}{\sqrt{2}} = 0.707. \tag{15}$$

The maximal power dissipated by friction, $P_{dis,\,max}$, which corresponds to a_{opt} is given by

$$P_{dis,\,max}(a_{opt}) = \frac{\omega F^2}{4}|H(j\omega)|. \tag{16}$$

3.3.3. Discussion

From the equations presented in the preceding section, it results that the maximal power dissipated arises from an intermediate situation between, on the one hand, a large friction force with a very small displacement (enough to ensure the relative motion at the friction interface); and on the other hand, a large displacement with a very small friction force (enough to ensure the contact between surfaces at the friction interface). This is in accordance with Eq. (9) which shows that, for a given frequency, if the normal force is large and thus the friction force is also large too, or, equivalently, the parameter a tends towards the magnitude of the excitation force F, the magnitude of displacement X tends towards zero. Consequently, in accordance with Eq. (12), the power dissipated also tends towards zero.

3.4. Modelling of the normal force generator

During relative motion, a normal force is applied to induce friction force at the interface of contact between the moving mass and the friction pads. In the semi-active device, piezoelectric stack actuators are used to apply the normal force. Each actuator is a multilayered piezoelectric actuator consisting of a number of piezoelectric elements in a stack. It is assumed that the electric field is applied only in the thickness direction of the piezoelectric elements (defined as direction "3") [22,23]. In this case, the linear constitutive equations are written as

$$\begin{aligned} \varepsilon_3 &= s_{33}^E \sigma_3 + d_{33} E_3, \\ D_3 &= d_{33}\sigma_3 + \varepsilon_3^T E_3, \end{aligned} \tag{17}$$

where ε_3, σ_3, D_3 and E_3 are, respectively, the strain, stress, electrical displacement (electrical charge per unit area) and the electric field (voltage per unit length). In addition, s_{33}^E, d_{33} and ε_3^T are the elastic compliance (the inverse of elastic modulus), the piezoelectric strain constant and the permittivity of the material, respectively.

For practical application, it might be useful to transform Eq. (17) such that physical quantities appear. These physical quantities are the displacement w, the force F, the applied voltage U_N and the electrical charge Q [24]. With the area of the actuator A and the thickness of each layer h, the following transformations are then introduced:

$$\varepsilon_3 = \frac{w}{h}, \quad \sigma_3 = \frac{F}{A}, \quad E_3 = \frac{U_N}{h}, \quad D_3 = \frac{Q}{A}. \tag{18}$$

If F_{ext} is the external force applied on a piezoelectric stack actuator with n thin layers of piezoelectric material, the strain is given by

$$\frac{w}{nh} = s_{33}^E \frac{F_{ext}}{A} + d_{33}\frac{U_N}{h}. \tag{19}$$

Eq. (19) can be rewritten in the following form:

$$F_{ext} = k_{pzt} w - F_{pzt}, \tag{20}$$

where $k_{pzt} = A/(nhs_{33}^E)$ and $F_{pzt} = k_{pzt} n d_{33} U_N = G_{pzt} U_N$ are, respectively, the stack actuator stiffness and the force generated by the piezoelectric stack actuator with $G_{pzt} = k_{pzt} n d_{33}$.

3.4.1. Free displacement

The free displacement, denoted w_l, is a function of the applied voltage obtained from Eq. (20) with $F_{\text{ext}} = 0$ and is given by

$$w_l = nd_{33}U_N = \frac{F_{\text{pzt}}}{k_{\text{pzt}}}. \tag{21}$$

With the maximal voltage applied, one can obtain the maximal free displacement which is one of the parameter needed to determine the range where the actuator can be operated. It should be emphasized that the free displacement is obtained in absence of any force along the actuator axis. However, more relevant for real applications, are the situations where external forces are applied. The next section discuss about the displacement under an external applied load.

3.4.2. Displacement under loading

In the semi-active device, under loading the stack actuator has to oppose to an external force. This one is measured and the equation of motion leads to

$$w = \frac{G_{\text{pzt}}U_N - F_{\text{ext}}}{k_{\text{pzt}}} \tag{22}$$

with the external force $F_{\text{ext}} = -k_e w$ where k_e is the equivalent stiffness of the device in the direction of external applied normal force.

The measured external force can be written explicitly as

$$F_{\text{ext}} = \frac{k_e}{k_e + k_{\text{pzt}}} G_{\text{pzt}}U_N. \tag{23}$$

For most applications, the relation between the displacement and the external load given by Eq. (22) can be considered linear [25]. The slope of this straight line is the inverse of the piezoelectric stack actuator stiffness k_{pzt} and the points where this line crosses the axis correspond, respectively, to the blocking force F_b (zero displacement) and to the maximal free displacement w_l (zero blocking force) for a given voltage applied.

As will be shown for the device, a preload F_0 is applied to ensure the contact between the surfaces of the moving mass and the frictions pads. The action of the preload results in compression of the equivalent stiffness of the actuator k_{pzt} and of the device itself k_e; the external force measured is then given by

$$F_{\text{ext}} = F_0 + \frac{k_e}{k_e + k_{\text{pzt}}} G_{\text{pzt}}U_N. \tag{24}$$

Eq. (24) shows that the modulation of the measured force around the preload F_0 depends on the piezoelectric stack actuator characteristics, the voltage applied and the stiffness of the device itself.

In order to verify that the actuator can fulfill the requirements for this application, the blocking force and the maximal free displacement which are obtained at the maximal applied voltage are properties to be considered. To validate the appropriateness of the actuator chosen, experimental displacement-force diagrams are plotted with the maximal blocking force on the x-axis and the maximal free displacement on the y-axis. The line connecting these two points delimits the actuator applicability region. Therefore, the preload and the applied voltage must be such that the external force in Eq. (24) remains in the applicability region of the actuator. Moreover, to avoid the sticking, the external force must also be such as the excitation force can allow the displacement of the moving mass.

4. Experimental validation of the semi-active device

4.1. Experimental setup

To validate the semi-active device concept, a prototype was designed and fabricated. Fig. 2 shows the semi-active device prototype which has the overall dimensions of 8.5 cm × 5.0 cm × 10.0 cm for a total weight of 1.20 kg. The device includes two flexible phosphor-bronze alloy blades with 0.41 mm thickness which are

attached to the moving mass made of stainless steel. The two flexible blades are clamped to the rigid frame. On each side of the moving mass, friction pads made from car brakes material are assembled. During relative displacement of the mass, normal forces provided by preload and two piezoelectric stack actuators on both sides of the moving mass, induce friction force at the interface contact between moving mass and frictions pads surfaces. To make sure that this normal force remains perpendicular to the motion of the moving mass and to correct possible misalignment due to the motion (coming, for example, from slight deviated blades), balls are inserted between the friction pads and the piezoelectric actuators.

For the characterization of the device, its lower part is blocked between the jaws of a vice used as a frame. Fig. 3 shows the device excited by a force generated by a shaker. Connection between the moving mass and the shaker produces the flexural displacement of the blades. During its displacement, the moving mass rubs on two friction pads located on both sides to provide, with the normal force applied, the friction force at the friction interface.

As shown in Fig. 3, an electromagnetic shaker (*B&K Type* 4809) with a power amplifier (*MB Dynamics Model SL600VCF*) is used to provide the excitation force. This force is measured using a force sensor (*PCB Piezotronics Model* 208*B*04: *sensitivity* 1.252 mV/N). Two accelerometers (*B&K* 4393: *sensitivity* 0.511 mV/m s^{-2}) are used for the measurement of the accelerations of the moving mass and of the friction pads. These two measurements acceleration allow to calculate the relative acceleration of the moving mass. The load cells used for normal force measurement are: (i) left load cell: *Intertechnology* with 3 klbs @ 3.376 mV/V; (ii) right load cell: *Sensortronics* with 1 klbs @ 3.539 mV/V. The PZT stack actuators used to apply the normal force are *BM*532 elements from *Sensor Technology Limited* and consist of 78 layers, each layer having 0.25 mm thickness. The maximal free displacement is about 9 μm for an applied voltage of 200 V. The maximal force generated in completely clamped conditions (blocking force) is 1200 N. The piezoelectric stack amplifier is a *PCB Piezotronics* 790 *Series*.

Force excitation sensor and accelerometers signals are conditioned with a charge amplifier (*PCB Piezotronics*) and the signals are then filtered by an elliptic low-pass filter with a cutoff frequency of 600 Hz (order 8, 8 poles and 6 zeros) from *Frequency Devices*, as an anti-aliasing filter. A Butterworth filter from *Rockland Series* 2000 *Filter* (8 poles, order 8) is used for filtering shaker and PZT stack actuators command signals.

The device characterization (identification of the device dynamic parameters and study of the device dissipative behavior) and friction model parameters identification are conducted under the *MATLAB/Simulink* environment. The controller is then implemented on *dSPACE* boards for real time signal processing; visualization and data acquisition are performed with the *ControlDesk* software.

4.2. Identification of the spring-mass-damper system parameters

Measurement of the excitation force and acceleration will allow to estimate the friction force from Eq. (1) provided that dynamic parameters (mass m, equivalent stiffness k and equivalent viscous damping c) are known. The present section focuses on this experimental identification. In Section 3.1, the dynamics of the

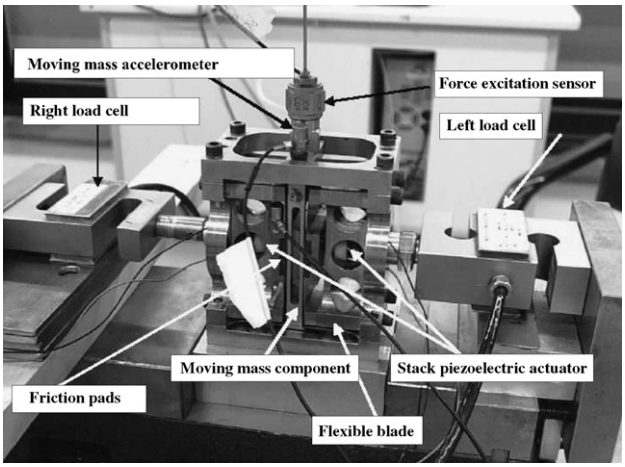

Fig. 2. Prototype of the semi-active friction device instrumented with sensors.

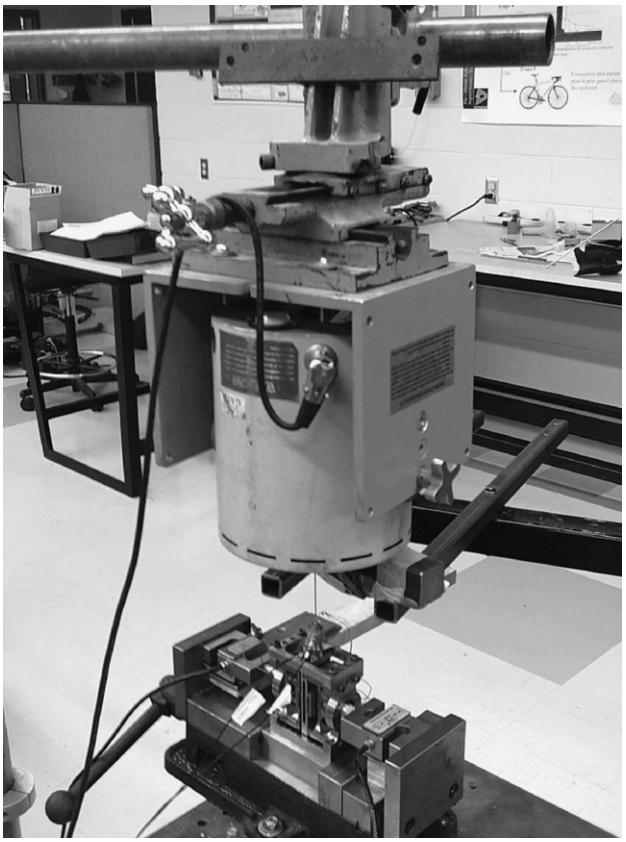

Fig. 3. Experimental setup for the device characterization and the friction study.

device without friction is represented by a second-order mass-spring-damping equation. The mass is determined by a simple weighting with a precision balance and one needs to obtain the transfer function for the determination of k and c. For the identification, measurement of the pseudo-random force applied by the shaker and the moving acceleration is done and data have been processed using MATLAB *Identification Toolbox*.

4.2.1. Results

Table 1 contains normalized parameters in the Laplace continuous domain. With $K_i = (1/m)$ and using the identified values of the natural frequency and damping coefficient in Eq. (3), the transfer function between the displacement and the excitation force can be rewritten such that it allows to find the static gain of this transfer function which corresponds to the inverse value of the equivalent stiffness of the semi-active device. The same value of k can be also calculated with the natural frequency with $k = \omega_n^2 m$. Table 1 presents all the identified parameters for the spring-mass-damper system.

4.3. Identification of the normal force generator parameters

The objective of this section is to validate the actuator "*Voltage– Displacement*" and "*Load– Displacement*" characteristics for various voltage applied to the actuator in order to determine its applicability region. Measurements are conducted to identify the actuator maximal free displacement w_l, blocking force F_b, stiffness k_{pzt} and force-voltage gain G_{pzt}. Fig. 4 shows a schematic diagram of the experimental setup used for the PZT stack actuator characterization. The PZT stack actuator is inserted between the rigid jaws of a vice for which tightening can be regulated with a lever arm. A load cell, installed in series with the actuator,

Table 1
Identification of the parameters of the moving mass system

$c/m = 2\zeta\omega_n = 31.13\,\mathrm{N/m\,s^{-1}}$
$\omega_n^2 = 7.643 \times 10^4\,\mathrm{rad/s^2}$
$K_i = \frac{1}{m} = 4.378\,\mathrm{kg^{-1}}$
Natural frequency $f_n = 45.0\,\mathrm{Hz}$
Damping ratio $\zeta = 5.63\%$
Mass $m = 0.228\,\mathrm{kg}$
Equivalent stiffness $k = 17.50\,\mathrm{kN/m}$
Equivalent damping coefficient $c = 7.10\,\mathrm{N/m\,s^{-1}}$

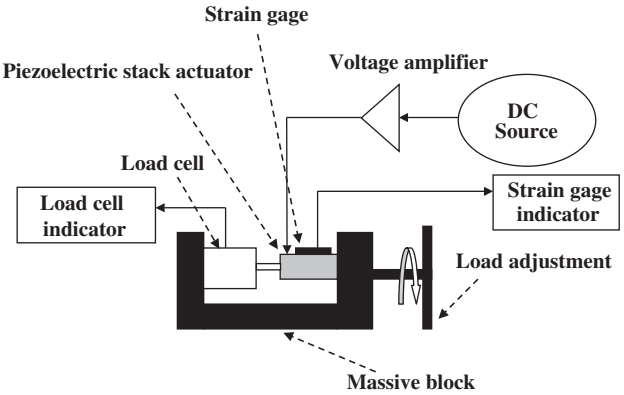

Fig. 4. Experimental setup for the PZT stack actuator characterization.

monitors the tightening force applied. The displacement is obtained from the measurement of the strain using a strain gage on the actuator. The voltage amplifier is used with the piezoelectric actuator.

Two series of measurements are conducted to identify the parameters of the piezoelectric actuators. A first series of measurements is conducted in free configuration, i.e. without the application of compression force on the PZT stack actuator. The voltage applied to the actuator varies from 0 to 200 V. The strain is measured to plot the free displacement versus applied voltage which will be compared with the curve provided by the manufacturer. A second series of measurements is conducted at constant load with various voltages applied to the actuator. For each voltage, strain is measured and corresponding displacement is calculated. When applied voltage is increased, the force applied by the actuator is increased consequently. But, since the measurement is conducted at constant load, the jaws of the vice are then loosened to reduce the force in order to retrieve the constant load under which the series of measurements is carried out. Tests were performed with voltage from 0 to 200 V with steps of 20 V and load from 0 to 250 lbs with steps of 25 lbs. With these measurements, the displacement–load curve for various applied voltages is obtained.

4.3.1. Analysis of the results

4.3.1.1. Free displacement. Fig. 5 illustrates the free displacement versus the applied voltage curve obtained. The curve is in agreement with the curve from the manufacturer although the maximal displacement at maximal voltage 200 V obtained is 8.00 μm while the manufacturer gives 9.50 μm.

4.3.1.2. Displacement under loading. Fig. 6 shows the displacement as a function of load obtained for various applied voltages. These curves are linear in accordance with Eq. (22). From the curve at 200 V, one can see that the maximal free displacement is $w_l = 8\,\mu\mathrm{m}$, the blocking force is $F_b = 900\,\mathrm{N}$, the stiffness is $k_{\mathrm{pzt}} = 120\,\mathrm{kN/mm}$ and the gain $G_{\mathrm{pzt}} = 4.5\,\mathrm{N/V}$ and then the applicability region of the PZT stack actuator is also determined by the area under this curve.

The stiffness value obtained is in accordance with those found in the literature for the PZT stack actuator [22]. The blocking force given by the manufacturer is 1200 N which is 25% greater than the experimental value obtained. The reason of this difference might be that the perfect clamped conditions could not be achieved experimentally for the PZT stack actuator because of the limited value of the vice stiffness.

In this study, the applicability region shows that the force applied by the PZT stack actuator can be modulated from 0 to 900 N. In practice however, the equivalent stiffness of the device in the direction of the normal force will limit the modulation around the preload in accordance with Eq. (23). Thus, a modulation with a maximal force smaller than 900 N is expected.

4.4. Identification of the friction model parameters

In order to evaluate the performance of the semi-active device in energy dissipation, tests with harmonic excitation force and constant voltage applied to the PZT stack actuator were performed. Therefore, for these tests, PZT stack actuator applies constant normal force and the setup is the same than the one presented in Fig. 3 and used for the identification of the moving mass system parameters.

Following the setup presented in Section 4.1 and in Fig. 3, a harmonic excitation force (with the frequency 50, 80 and 100 Hz and phase shift $\gamma = 0$) is applied, a preload (90 and 100 N) is also applied and various constant voltages U_N from -200 to $+200$ V are applied to the PZT stack actuators which corresponds to

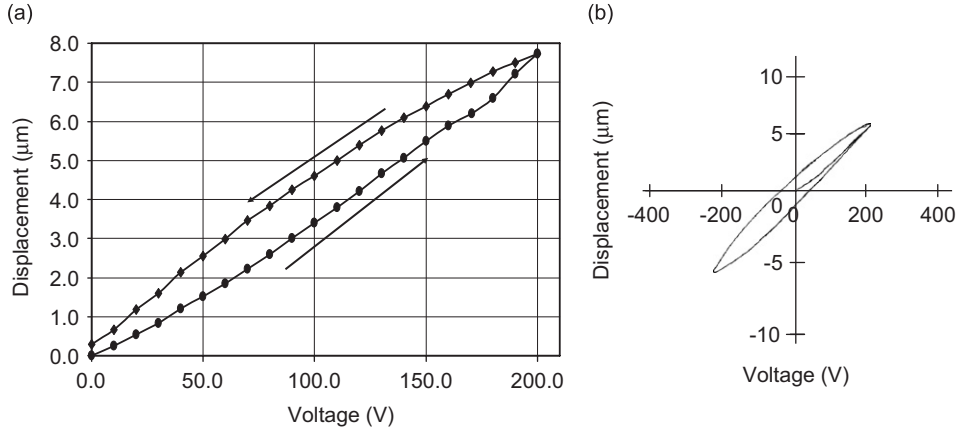

Fig. 5. Experimental (a) and manufacturer (b) free displacement characteristics.

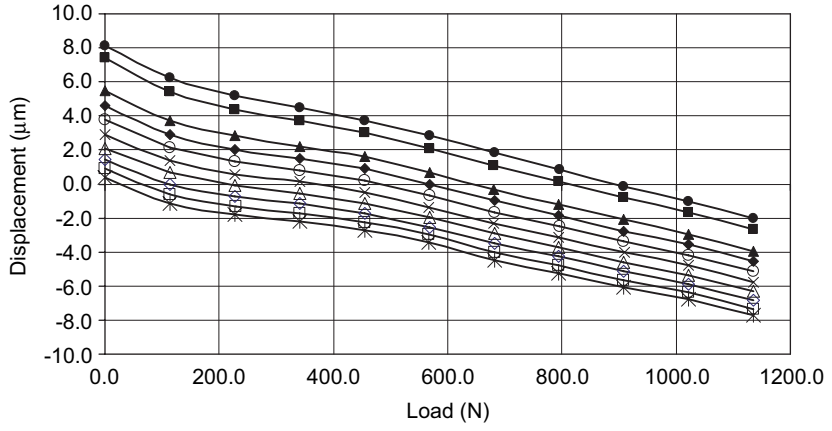

Fig. 6. Displacement-load characteristic for various voltage U_N applied. ✻ $U_N = 0$ V; □ $U_N = 20$ V; ◇ $U_N = 40$ V; △ $U_N = 60$ V; × $U_N = 80$ V; ○ $U_N = 100$ V; ◆ $U_N = 120$ V; ▲ $U_N = 140$ V; ■ $U_N = 180$ V; • $U_N = 200$ V.

various normal forces. So, the analysis is conducted to visualize the influence of increasing the normal force on the friction force and on the displacement of the moving mass, and therefore on the energy dissipated.

4.4.1. Analysis of the results

Table 2 presents the experimental results for the preload of 90 N and excitation frequency of 80 Hz, and presents measurements of normal forces (right F_{nR} and left F_{nL}), root-mean-square (rms) values of the relative displacement x_{rms}, and also calculated values of the energy dissipated per cycle E_{dis} and corresponding dissipated power P_{dis}.

Although the simplified Coulomb friction model is adopted in theoretical development, to take into account all the phenomena present in the real friction force, the energy dissipated is estimated from Eq. (11) by numerical integration to compute the area inside the friction force–displacement curve which represents the energy dissipated by cycle. So, during the experimental test, the excitation force and the acceleration of the moving mass are measured. The velocity and the displacement are then obtained by integrating the measured acceleration and the friction force is estimated using Eq. (1) put in the following form: $F_f(t) = m\ddot{x}(t) - F_{\text{exc}}(t) - c\dot{x}(t) - kx(t)$. The friction force–displacement plot can thus be obtained and the area under the curve is calculated to provide the estimated value of the energy dissipated.

4.4.1.1. Friction law as a function of applied voltage. Fig. 7(a) shows the friction force as a function of the velocity where the friction force is estimated from Eq. (1) and the relative velocity is obtained by integration of acceleration measurements for various voltages applied to the PZT stack actuators. For applied voltages of 0, 100 and 200 V, respectively corresponding to normal forces of 90.4, 102.4 and 114.20 N, the friction force increases in the vicinity of zero velocity. This is illustrated in the Stribeck effect. The curve for the friction force for applied voltage of 100 V shows that the friction force remains almost constant above a velocity of 0.02 m/s. This velocity corresponds to the transition from the sticking to the sliding motion which is considered as the Stribeck velocity. For the 200 V voltage curve, the effect on sticking motion is dominant such that the sliding remains in the region where the Stribeck effect is important.

One can state that for the applied voltages of 0, 100 and 200 V, the *friction force– velocity* plot combines the Coulomb friction with the viscous friction and the Stribeck effect at low velocities. However, for the lower normal forces 73.15 and 82.60 N corresponding, respectively to voltages of −100 and −200 V the curve for friction force as a function of velocity does not follow the same behavior for the friction model. This is due to the fact that, with smaller normal force, contact between the moving mass and the friction pads is not as good at the friction interface.

From the curve of the friction force as a function of velocity at applied voltages of 100 and 200 V, the Coulomb friction force parameter is estimated at $F_c \approx 42$ N for 100 V and $F_c \approx 55$ N for 200 V, which is equivalent to an average dynamic coefficient of friction $\mu \approx 0.5$.

4.4.1.2. Power dissipated as a function of the applied voltage. Fig. 7(b) shows the friction force as a function of the displacement for various applied voltages. The area under each curve represents the energy dissipated per cycle at the given voltage and the corresponding power dissipated can be calculated.

A negative voltage applied to the PZT stack actuators (from 0 to −200 V) reduces the normal force because the actuator force is opposed to the preload (values are, respectively, 73 N corresponding to reduction of 17 N

Table 2
Experimental results for the constant applied voltage to the PZT stack actuators (preload = 90 N)

f (Hz)	U_N (V)	$F_{NR\ \text{mean}}$ (N)	$F_{NL\ \text{mean}}$ (N)	$F_{N\ \text{mean}}$ (N)	x_{rms} (μm)	E_{dis} (mJ)	P_{dis} (W)
	−200.00	75.80	70.50	73.15	339.00	9.90	0.80
	−100.00	84.20	80.90	82.60	271.00	23.80	1.91
80	0.00	92.60	90.40	91.50	201.00	29.20	2.33
	+100.00	103.70	102.40	103.30	102.00	22.30	1.80
	+200.00	115.20	114.70	114.94	39.40	10.60	0.85

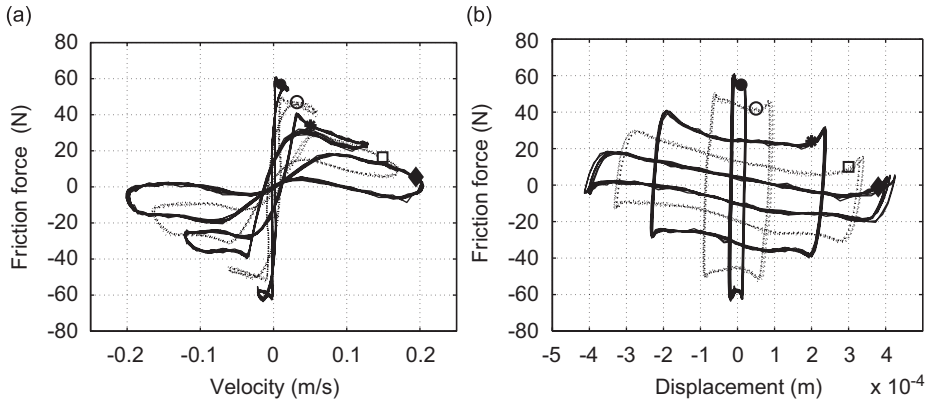

Fig. 7. Friction force versus velocity (a) and versus displacement (b) for various voltage U_N applied. ◆ $U_N = -200$ V; □ $U_N = -100$ V; ∗ $U_N = 0$ V; ◯ $U_N = 100$ V; • $U_N = 200$ V.

for −200 V and 91.5 N corresponding to reduction of 0 N for 0 V). The reduction of the normal force releases the friction pads from the moving mass surfaces. Therefore, the friction force is then reduced and the displacement amplitude increases because of the reduction in the resistance to the motion. This can be observed on the corresponding curve of friction force as a function of the displacement for voltages applied of −100 and −200 V.

A positive voltage applied to the PZT stack actuators (from 0 to +200 V) increases the normal force because the actuator force is in the same direction as the preload (values are respectively 91.5 N corresponding to an increase of 0 N for 0 V and 114.5 N corresponding to an increase of 23.0 N for +200 V). An increase of the normal force leads to an increase of the friction force and, therefore to the reduction of the relative displacement as observed for 0 V, +100 V and +200 V in the curves of friction force as a function of the displacement.

From the analysis above, it appears that the two effects, i.e. increasing the normal force to increase the friction force and to reduce the displacement or reducing the normal force to reduce the friction force and increase the displacement, both have influence on the area under the curve for the friction force as a function of displacement, corresponding to the energy dissipated per cycle. Thus, to obtain a large dissipated power, it is necessary to make a compromise between a large normal force which leads to a small displacement or a small normal force which leads to a large displacement. The experimental analysis of this compromise will be presented in Section 4.5 for the determination of the optimal dissipated region with the constant voltage applied to the PZT stack actuators.

4.4.1.3. Stick-slip phenomenon as a function of the applied voltage. Fig. 8(a) shows the time-domain history of acceleration, velocity and displacement of the moving mass for an applied voltage of +100 V. With the increase of the voltage applied to the PZT stack actuators, acceleration is almost zero in some regions leading to almost constant speed and consequently linear displacement. These regions correspond to the appearance of the stick-slip phenomenon in the vicinity of zero velocity where the dynamic friction effect has an important impact on friction force. Fig. 8(b) illustrates that the stick-slip phenomenon appears when the absolute value of the friction force is greater than the absolute value of the excitation force. Fig. 9 illustrates also the stick-slip phenomenon on the phase diagram with the region of constant velocity for the applied voltage from −200 to +200 V at excitation frequency of 80 Hz. From Fig. 9(a), one can observe that for applied voltage from −200 to 0 V, corresponding to normal force from 73 to 91 N, the stick-slip phenomenon does not appear while it does for applied voltage greater than 0 V when the friction force becomes important in accordance with the friction law presented in Fig. 7. During the stick-slip, there is no relative motion at the friction interface and therefore there is no power dissipated. A proper choice of the instantaneous normal force can avoid this stick-slip phenomenon and thus improve energy dissipated by friction.

4.4.1.4. Impact of stick-slip phenomenon on power dissipated. The analysis of the curves presented in Fig. 10 for friction force as a function of the velocity and friction force as a function of the displacement allows to

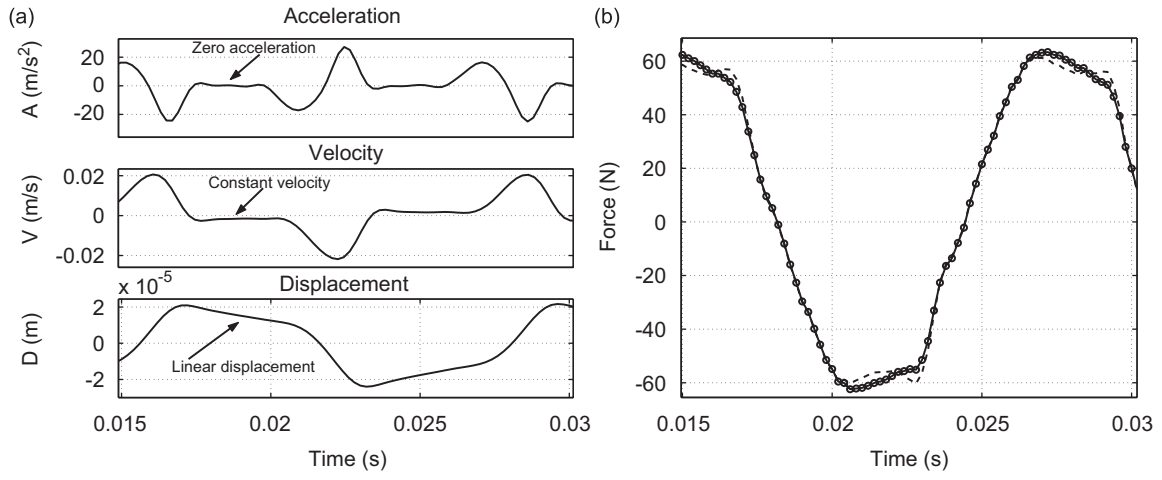

Fig. 8. Stick-slip phenomenon (a) and excitation (○) and friction(−−) forces (b) for $U_N = 200\,\mathrm{V}$ ($F_c \approx 55\,\mathrm{N}$).

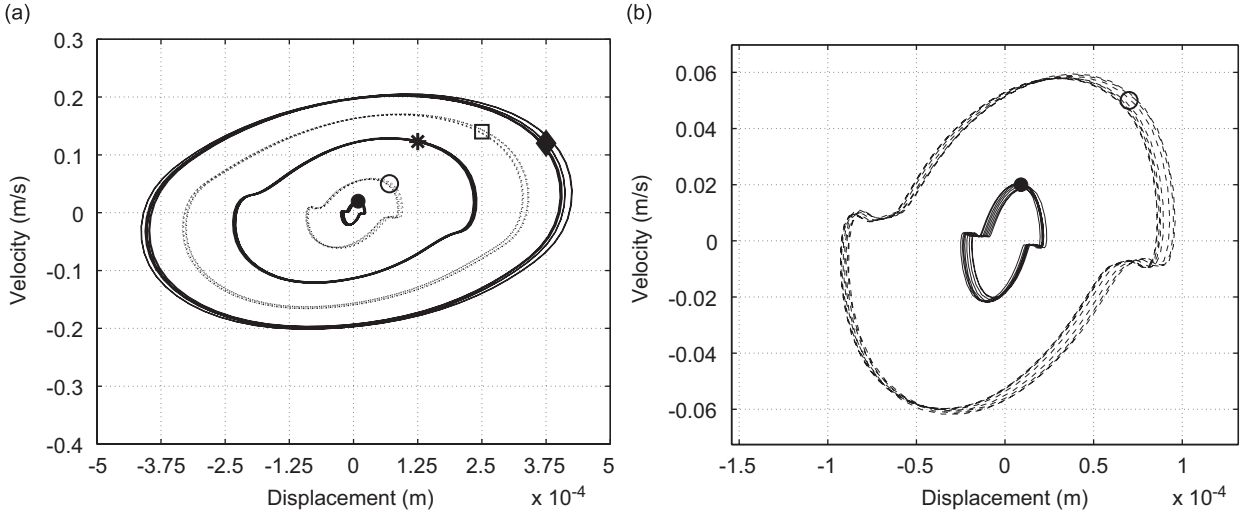

Fig. 9. Phase diagram and zoom on $U_N = 100\,\mathrm{V}$ ($F_c \approx 42\,\mathrm{N}$) (a) and $U_N = 200\,\mathrm{V}$ ($F_c \approx 55\,\mathrm{N}$) (b). ◆ $U_N = -200\,\mathrm{V}$; □ $U_N = -100\,\mathrm{V}$; ∗ $U_N = 0\,\mathrm{V}$; ◯ $U_N = 100\,\mathrm{V}$; • $U_N = 200\,\mathrm{V}$.

validate the results and the conclusions found in the literature on the impact of the stick-slip phenomenon on energy dissipated by friction. Fig. 10(a) shows regions where there is: (i) dissipation of energy corresponding to the positive power dissipated, i.e. $P_{\mathrm{dis}} = F_f\dot{x} > 0$ with $F_f > 0$ *and* $\dot{x} > 0$ or $F_f < 0$ *and* $\dot{x} < 0$; (ii) restitution of energy corresponding to the negative value of the power dissipated, i.e. $P_{\mathrm{dis}} = F_f\dot{x} < 0$ with $F_f > 0$ *and* $\dot{x} < 0$ or $F_f < 0$ *and* $\dot{x} > 0$ [26]. The energy is thus dissipated when the friction force has same sign as the velocity.

The stick-slip reduces the power dissipated because of the absence of sliding during the sticking. The friction force magnitude decreases immediately prior to the slip-to-stick or to the stick-to-slip transition while it remains almost constant during the sliding. This observation confirms the one made by Liang and Feeny in their friction setup [27].

Fig. 10(b) shows the curve of friction force as a function of the displacement with the area under the curve corresponding to the energy dissipated per cycle of oscillation. The slope in the sticking period gives the stiffness of the contact joint which corresponds to the bristles stiffness of the LuGre model [19,28].

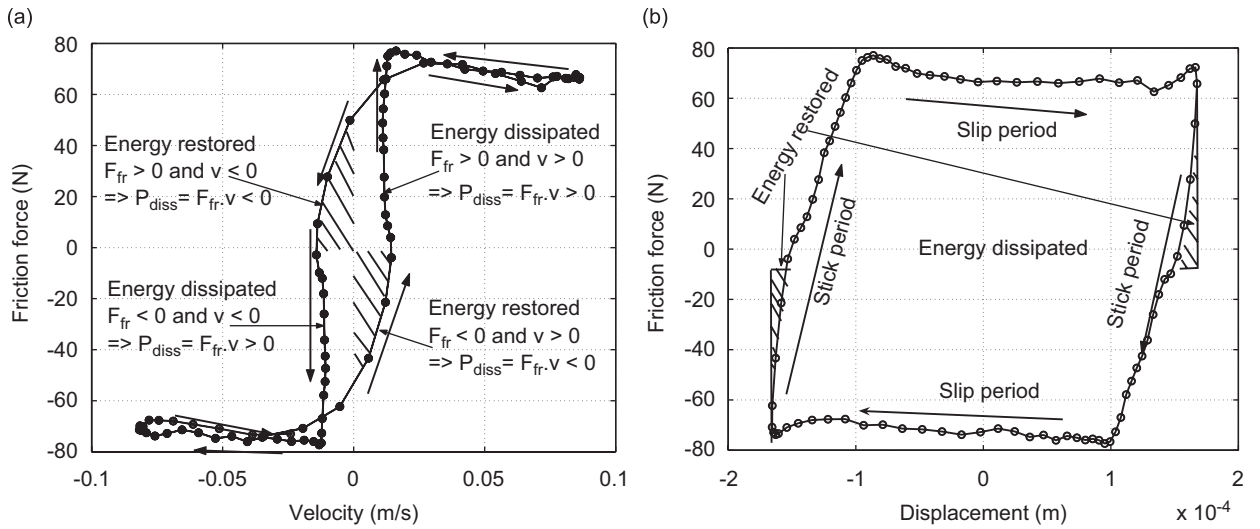

Fig. 10. Friction force versus velocity (a) and displacement (b) for $F_{exc} = 80\,N$ and $F_N = 115\,N$ at $f = 60\,Hz$.

Table 3
Experimental results for the optimal dissipation for the constant applied voltage to the PZT stack actuators (preload = 100 N)

f (Hz)	U_N (V)	$F_{N\,mean}$ (N)	$F_{fr\ rms}$ (N)	x_{rms} (μm)	P_{dis} (W)	P_{inj} (W)
	−200.00	84.36	15.51	315.00	2.12	3.20
	−150.00	88.54	19.86	279.00	2.49	3.34
	−100.00	92.61	23.87	246.00	2.64	3.30
	−50.00	97.54	28.30	218.00	2.77	3.29
80	0.00	102.74	32.70	186.00	2.71	3.10
	+50.00	108.77	38.52	141.00	2.40	2.61
	+100.00	117.20	43.82	92.30	1.84	1.92
	+150.00	129.54	52.58	17.10	0.44	0.45
	+200.00	140.04	53.94	0.20	0.00	0.00

4.5. Experimental determination of optimal dissipation

In Section 3.3.2 it was shown that the maximal power dissipated is found for $a_{opt}/F = 1/\sqrt{2} = 0.707$. In this section, measurements are performed to corroborate the theoretical prediction for the excitation force frequencies 80 and 100 Hz; the preloads 90 and 100 N; and the applied voltage to stack actuator of −200, −150, −100, −50, 0, +50, +100, +150 and +200 V.

4.5.1. Analysis of the results

Table 3 presents the measurement for the case of $f = 80\,Hz$ and the preload of 100 N.

4.5.1.1. Power injected and power dissipated. For the various applied voltages, Fig. 11 illustrates (a) the excitation force as a function of displacement and (b) the friction force as a function of displacement. The area under each curve, corresponds, respectively, to the energy injected and to the energy dissipated per cycle. In accordance with the results in Table 3, for applied voltages such that $U_N > 0$, the equality between the injected and the dissipated power is respected (with 10% precision). But, for $U_N < 0$ the equality is not respected because the friction force is not effective, as shown in Fig. 12(b), due to the small normal force. The power injected is thus dissipated by mechanisms other than that modelled by friction.

4.5.1.2. Optimal dissipation. Fig. 13 illustrates the power dissipated as a function of normalized normal force for various excitation frequencies and preloads. These curves show the existence of the optimal normal force which leads to the maximal power dissipated.

The normalization of the normal force is performed by dividing each normal force with the estimated normal force which causes the blocking of motion. It appears in these curves that the maximal power dissipated is obtained for the parameter $a_{\text{norm opt}} = 1/\sqrt{2} = 0.707$, which confirms the theoretical prediction. Thus, for a given excitation force of amplitude F at a frequency ω, an increase of the normal force and consequently of the friction force, results in an increase of the power dissipated up to an optimal value of the normal force corresponding to the maximal power dissipated. Above the optimal normal force, if the normal force continues to increase, the friction will also increase. Consequently, the resistance to the motion increases and the moving mass tends to stick, resulting in a reduction of the power dissipated.

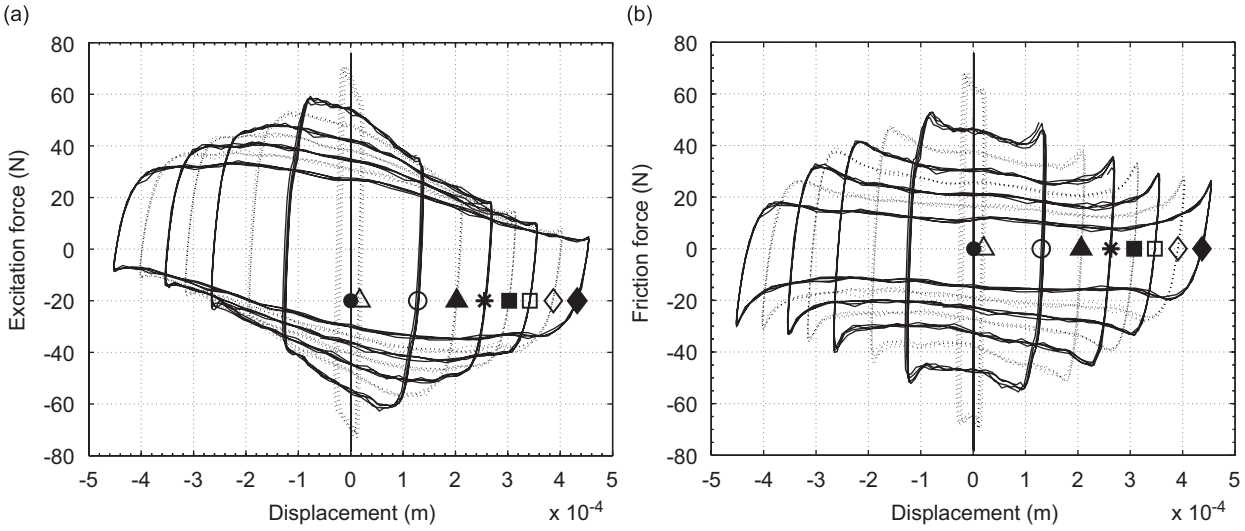

Fig. 11. Excitation force (a) and friction force (b) versus displacement for various voltage U_N at frequency $f = 80$ Hz. ◆ $U_N = -200$ V; ◇ $U_N = -150$ V; □ $U_N = -100$ V; ■ $U_N = -50$ V; ∗ $U_N = 0$ V; ▲ $U_N = 50$ V; ◯ $U_N = 100$ V; △ $U_N = 150$ V; • $U_N = 200$ V.

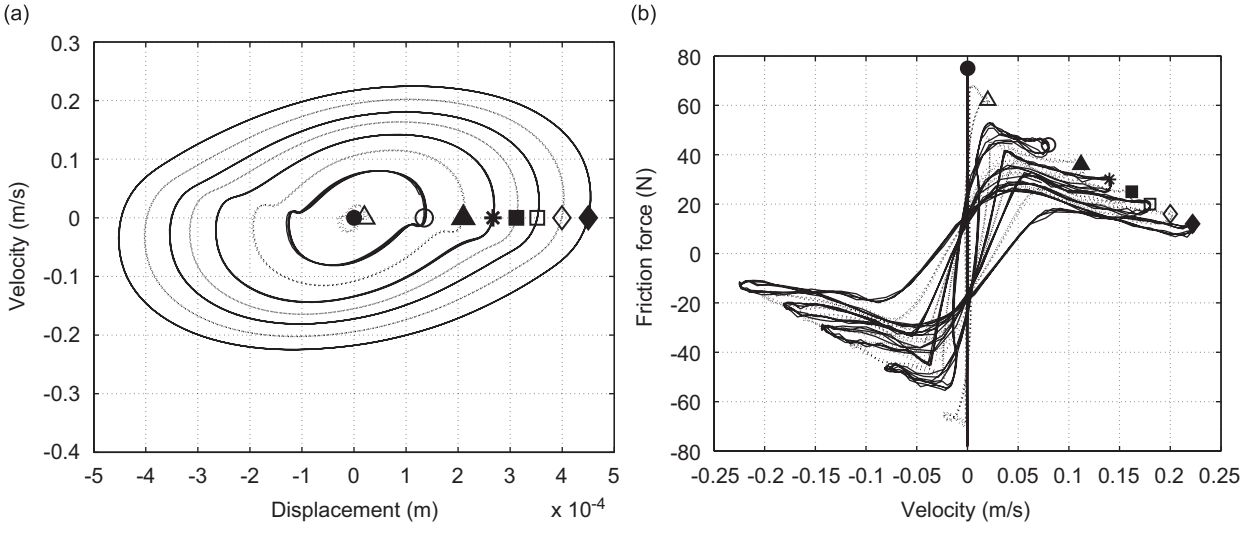

Fig. 12. Phase diagram (a) and friction force versus velocity (b) for various voltage U_N. ◆ $U_N = -200$ V; ◇ $U_N = -150$ V; □ $U_N = -100$ V; ■ $U_N = -50$ V; ∗ $U_N = 0$ V; ▲ $U_N = 50$ V; ◯ $U_N = 100$ V; △ $U_N = 150$ V; • $U_N = 200$ V.

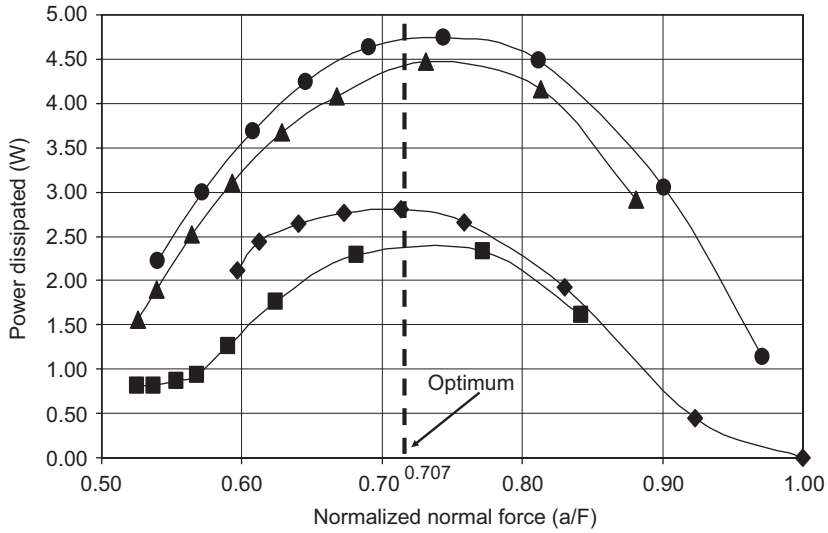

Fig. 13. Power dissipated versus normalized normal force. ■ $f = 80\,\text{Hz}$, $F_N = 90\,\text{N}$; ◆ $f = 80\,\text{Hz}$, $F_N = 100\,\text{N}$; ▲ $f = 100\,\text{Hz}$, $F_N = 90\,\text{N}$; • $f = 100\,\text{Hz}$, $F_N = 100\,\text{N}$.

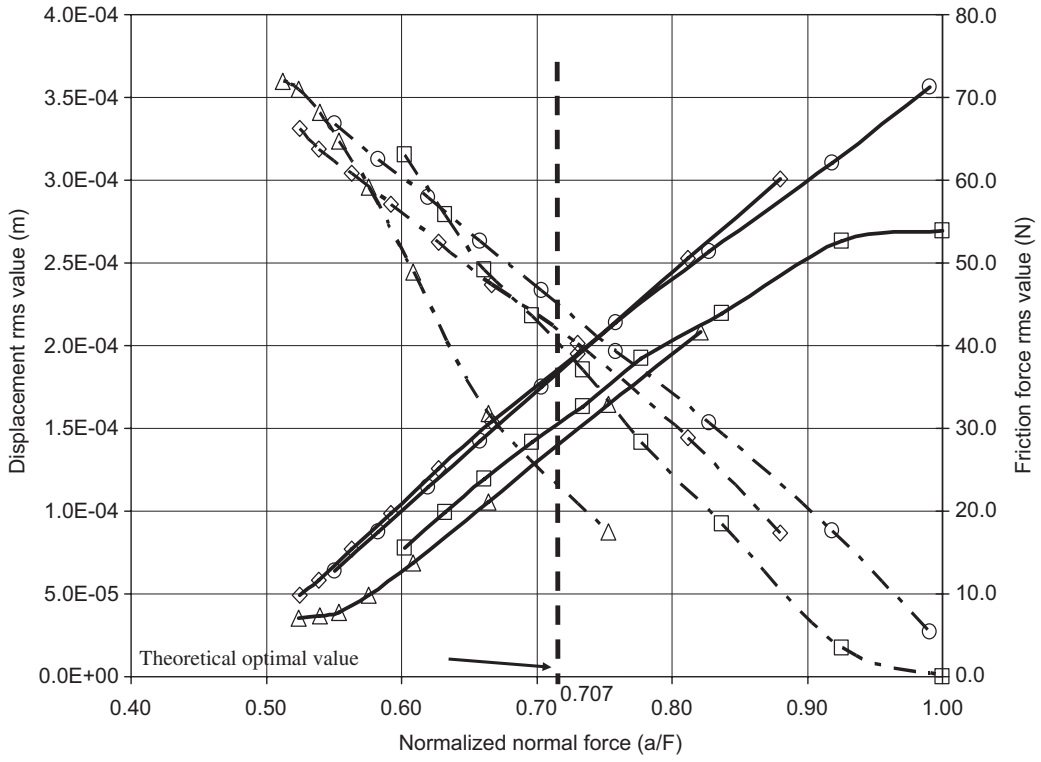

Fig. 14. Displacement (solid line) and friction force (dash-dot line) rms value versus normalized normal force for various frequencies and normal forces. △ $f = 80\,\text{Hz}$, $F_N = 90\,\text{N}$; ◇ $f = 100\,\text{Hz}$, $F_N = 90\,\text{N}$; □ $f = 80\,\text{Hz}$, $F_N = 100\,\text{N}$; ○ $f = 100\,\text{Hz}$, $F_N = 100\,\text{N}$.

It appears that it is necessary to find the proper combination of normal force and displacement to obtain an optimal power dissipation. Theoretical development in Section 3.1 and experimental results presented above, have shown that this situation corresponds to a normal force equal 0.707 times the normal force corresponding to the blocking motion.

Fig. 14 presented the rms value of the displacement and of the friction force as a function of the normalized normal force. On the right side of the optimal region, small displacements with a large friction force are observed. This case corresponds to the excitation frequency of 100 Hz and applied voltage of +200 V where the normal force is 150 N which leads to the friction force of 70 N and the displacement smaller than 5×10^{-5} m. Thus, the normal force being very large, the motion is blocked and no power is dissipated. On the left of the optimal region, displacement is large and the normal force and the corresponding friction force are small. This is the case with the excitation frequency of 100 Hz and the applied voltage of −200 V where, the normal force is 85 N with 12 N as the corresponding friction force but the displacement is 3.5×10^{-4} m. In this case, the motion tends towards free motion without the friction force and thus the power dissipated by friction also tends towards zero.

5. Conclusions

A semi-active device was presented for vibration control using energy dissipation by dry friction at contact surfaces. The components of the device include a moving mass, flexure elements, friction pads and two piezoelectric elements to generate the normal force. It was shown that high normal force can lead to stiction that can cancel the friction effect while low normal force can lead to the absence of contact between the friction surfaces, therefore leading to no dissipation of energy.

Simple analytical models were presented to describe the dynamic behavior of the device. A second-order model was used for the spring-mass-damper system. The LuGre model is first proposed to describe the dry friction force in the system. In order to allow for an analytical expression for the optimal normal force for maximal energy dissipation, the LuGre model is reduced to a Coulomb model. It is shown that there exist an optimal value for the normal force given by $F_N = \pi F/(4\sqrt{2}\mu)$ where F is the external force applied and μ is the dynamic coefficient of friction. The normal force generator is a piezoelectric stack actuator and is modelled by the piezoelectric constitutive equations coupled with the dynamics of the device.

An experimental setup is then presented to identify the parameters of the spring-mass-damper, force generator and dry friction models. The procedures for the measurement of the parameters are detailed. The experimental measurements allow in particular to validate the friction model and to illustrate the stick-slip phenomenon and to calculate the power dissipated by the device as a function of the applied voltage.

Then, to validate the analytical prediction of an optimal normal force, measurements are conducted on the device under different excitation frequency, preload and applied voltage to the actuators. The experimental results confirm the existence of an optimal normal force for maximal energy dissipation.

Control algorithms are currently being developed to adjust the normal force so that maximal energy dissipation is achieved under normal operating conditions. Future work also includes the miniaturization of the device using MEMS technologies.

Acknowledgments

This work was supported by the National Science and Engineering Research Council (NSERC) and by the Network of Centres of Excellence AUTO21, Canada.

References

[1] J. Lane, Control of Systems Using Semi-active Friction Damping, PhD Thesis, Georgia Institute of Technology, 1992.
[2] N. McClamroch, H. Gavin, Electrorheological dampers and semi-active structural control, *Proceedings of 34th Conference on Decision and Control*, New-Orleans, LA, 1994, pp. 3528–3533.
[3] J. Lane, S.L. Dickerson, Contribution of passive damping to the control of flexible manipulators, *Proceedings of the ASME International Computers in Engineering Conference*, Las Vegas, NV, 1984, pp. 175–180.
[4] A. Ferri, B.S. Heck, Semi-Active suspension using dry friction energy dissipation, *Proceedings of the 1992 American Control Conference*, Chicago, IL, June 1992, pp. 31–35.
[5] L. Gaul, R. Nitsche, Friction control for vibration suppression, *Mechanical Systems and Signal Processing* 14 (2000) 139–150.
[6] L. Gaul, R. Nitsche, Lyapunov design of damping controllers, *Journal of Applied Mechanics* 72 (2003) 865–874.

[7] O. Durmaz, W.C. Clark, D.S. Bennett, J.S. Paine, M.N. Samuelson, Experimental and analytical studies of a novel semi-active piezoelectric coulomb damper, *Proceedings of the SPIE Smart Structures and materials 2002*, Vol. 4697, San Diego, CA, 2002, pp. 258–273.
[8] M. Lorenz, B. Heimann, J.G. Tschimmel, V. Hartel, Applying semi-active friction damping to elastic supports for automotive applications, *Proceedings of the IEEE ASME International Conference on Advanced Intelligent Mechatronics*, Kobe, Japan, 2003.
[9] M. Unsal, C. Niezrecki, C. Crane III, A new semi-active piezoelectric-based friction damper, *Proceedings of the SPIE Smart Structures and Materials 2003*, Vol. 5052, San Diego, CA, 2003, pp. 413–420.
[10] B. Armstrong-Hélouvry, P. Dupont, C. Canudas de Wit, A survey of models, analysis tools and compensation methods for the control of machines with friction, *Automatica* 30 (1994) 1083–1138.
[11] P. Buaka, P. Micheau, P. Masson, First steps in the development of a semi-active friction device to reduce vibration by energy dissipation, *Proceedings of the Second Canada– US CanSmart Workshop Smart Materials and Structures*, Montreal, QC, Canada, 2002, pp. 73–82.
[12] P. Buaka, P. Micheau, P. Masson, Development of a semi-active device to reduce vibration by energy dissipation in dry contact: experimental results on the first prototype, *Proceedings of 6th CanSmart Meeting International Workshop Smart Materials and Structures*, Montreal, QC, Canada, 2003, pp. 381–390.
[13] P. Buaka, P. Micheau, P. Masson, Development of a semi-active friction device to reduce vibration by energy dissipation: concept and design, *Proceedings of SPIE 2003 Smart Structures and Materials and Non-destructive Evaluation for Health Monitoring and Diagnostics*, Vol. 5056, San Diego, CA, 2003, pp. 603–614.
[14] P. Buaka, P. Micheau, P. Masson, Experimental validation of a semi-active friction device, *Proceedings of SPIE 2004 Smart Structures and Materials and Non-destructive Evaluation for Health Monitoring and Diagnostics*, Vol. 5390, San Diego, CA, 2004, pp. 347–358.
[15] P. Buaka, Development of a Semi-active Device for the Reduction of Vibrations in Mechanical Structures by Dry Friction Energy Dissipation, PhD Thesis, Université de Sherbrooke, 2005, (in French).
[16] P. Buaka, P. Micheau, P. Masson, Optimal energy dissipation in a semi-active friction device, *Journal of the Acoustical Society of America* 117 (4) (2005) 2602 *Presented at the 149th Meeting of the Acoustical Society of America*, Vancouver, Canada, 2005.
[17] A. Nashif, D. Jones, J. Henderson, *Vibration Damping*, Wiley, New York, 1985.
[18] P. Dupont, P. Kasturi, A. Stokes, Semi-active control of friction dampers, *Journal of Sound and Vibration* 202 (1997) 203–218.
[19] C. Canudas de Wit, H. Olsson, K.J. Astrom, A new model for control of systems with friction, *IEEE Transactions on Automatic Control* 40 (1995) 419–425.
[20] R.H.A. Hensen, Controlled Mechanical Systems with Friction, PhD Thesis, Technische Universiteit Eindhoven, 2002.
[21] C. Chaidez, Contribution to the Assessment of the Efficiency of Friction Dissipators for Seismic Protection of Building, PhD Thesis, Universitat Polytecnica de Catalunya, 2003.
[22] V. Giurgiutiu, C.A. Rogers, Power and energy characteristics of solid-state induced-strain actuators for static and dynamic application, *Journal of Intelligent Material Systems and Structures* 8 (1997) 738–750.
[23] W.K.W. Heverly, E.D. Smith, Dual-stack piezoelectric device with bidirectional actuation and improved performance, *Journal of Intelligent Material Systems and Structures* 15 (2004) 565–574.
[24] E.L. Colla, T. Monita, Piezoelectric technology for active vibration control, in: N. Setter (Ed.), *Piezoelectric Materials in Devices: Extended Reviews on Current Emerging Materials*, *Technology and Applications*, Ceramics Laboratory, EPFL Swiss Federal Institute of Technology, 2002, pp. 123–154 (Chapter 6). ISBN 2-9700346-0-3.
[25] C. Dhananjay, K.S. Inderjit, Design of high force, high displacement actuators for helicopter rotors, *Smart Material and Structures* 5 (1996) 58–67.
[26] P.S. Kasturi, On the Identification and Haptic Display of Friction, PhD Thesis, Stanford University, 2000.
[27] J.W. Liang, B.F. Feeny, Identifying coulomb and viscous friction in forced dual-damped oscillators, *Journal of Vibration and Acoustics, Transactions of the ASME* 126 (2004) 118–125.
[28] J.W. Liang, B.F. Feeny, Dynamical friction behavior in a forced oscillator with a compliant contact, *Journal of Applied Mechanics* 65 (1998) 250–257.